Electronic Supplementary Information for MS:

Modulating Methane Storage in Anionic Nano-porous MOF Materials via Post-synthetic Cation Exchange Process

Kamran Akhbari and Ali Morsali*

Department of Chemistry, Faculty of Sciences, Tarbiat Modares University, P.O. Box 14115-175, Tehran, Islamic Republic of Iran.

Contents

Materials and Physical Techniques

All reagents for the Syntheses and analysis were commercially available and used as received. Microanalyses were carried out using a Heraeus CHN-O- Rapid analyzer. The amounts of metal ions in each sample were measured by ICP analyses. Melting points were measured on an Electrothermal 9100 apparatus and are uncorrected. IR spectra were recorded using Perkin-Elmer 597 and Nicolet 510P spectrophotometers. ^{1}H-NMR spectra were measured in d_6-DMSO with a BRUKER DRX-500 AVANCE spectrometer at 500 MHz. The thermal behavior was measured with a PL-STA 1500 apparatus with the rate of 10 $^oC.min^{-1}$ in a static atmosphere of nitrogen. Crystallographic measurements were made using a Bruker APEX area-detector diffractometer. The intensity data were collected using graphite monochromataed Cu–K_α radiation. The structure was solved by direct methods and refined by full–matrix least–squares techniques on F^2. The molecular structure plot and simulated XRD powder pattern based on single crystal data were prepared using Mercury software.[1] X-ray powder diffraction (XRD) measurements were performed using a Philips diffractometer of X'pert company with monochromated Cu-k_α radiation. The samples were characterized with a scanning electron microscope (SEM) (Philips XL 30) with gold coating. N_2 (at 77 K) and low-pressure CH_4 (at 298 K) physisorption isotherms were measured up to 1 bar using approximately 0.2 g sample on a volumetric BELSORP-max apparatus by high-purity gases (N_2: 99.999% and CH_4: 99.5%). Prior to the N_2 adsorption measurement, the sample was degassed under reduced pressure at 373 K. For low-pressure CH_4 measurment, after each sample was set in the apparatus, the adsorbed molecules in the pore and on the surface were removed by heating under reduced pressure up to at 373 K.

(1) Mercury 1.4.1, Copyright Cambridge Crystallographic Data Centre, 12 Union Road, Cambridge, CB2 1EZ, UK, **2001-2005**.

Synthesis of $[HDMA]_2[Zn_2(BDC)_3(DMA)_2]$.6DMF (1) and preparation of its single crystals

White powders of **1** were synthesized by dissolving 1 mmol (0.166 g) 1,4-benzenedicarboxylic acid (H_2BDC) and 1 mmol (0.297 g) $Zn(NO_3)_2$,$6H_2O$ in 10 ml DMF. After preparation a transparent solution by stirring at room temperature, it was

transferred to the teflon-lined steel autoclave and heating at 180 ºC. After 48 hours, the teflon-lined steel autoclave was slowly cooled to room temperature with the rate of 0.1 °C.min^{-1}. The resulting product was washed with DMF and store in it, d.p. = above 300 °C, yield: 0.068 g, 22 % based on final product, Anal. calc. For $C_{25}H_{42}N_5O_9Zn$: C, 48.27; H, 6.82; N, 11.26 found; C, 48.19; H, 6.89; N, 11.19 %. In order to preparation of compound **1** single crystal, we repeated the above reaction by adding 0.5 mmol (0.064 g) terephthalodinitrile to the initial reaction precursors, d.p. = above 300 °C, yield: 0.075 g, 24 % based on final product, Anal. calc. For $C_{25}H_{42}N_5O_9Zn$: C, 48.27; H, 6.82; N, 11.26 found; C, 48.31; H, 6.85; N, 11.32 %. In addition to elemental analyses, IR spectra of these two compounds (Figure S1) and their XRD patterns (Figure S2a-c) approved that they are the same compounds. CCDC 896830 contains the supplementary crystallographic data for this anionic MOF. Since the yield of this reaction is low, we attempted to syntheses this anionic MOF in large scale to consider its cation exchange process and obtain enough MOF materials for studying their gas adsorption capacities. Thus initially we performed the above reaction under reflux condition, but the XRD pattern of the product (Figure S2d) was not match with that of **1** (Figure S2a,c), d.p. = above 300 °C, Anal. calc. For $C_{25}H_{42}N_5O_9Zn$: C, 48.27; H, 6.82; N, 11.26 found; C, 35.21; H, 2.39; N, 4.12 %. Finally we synthesized MOF material of **1** by dissolving 60 mmol (9.960 g) 1,4-benzenedicarboxylic acid (H_2BDC), 60 mmol (17.820 g) $Zn(NO_3)_2$,$6H_2O$ and 30 mmol (3.840 g) terephthalodinitrile in 100 ml DMF. The mixture was transferred to a large teflon-lined steel autoclave and heating at 120 ºC. After 48 hours, the teflon-lined steel autoclave was slowly cooled to room temperature with the rate of 0.1 °C.min^{-1}. The crystalline product was washed with DMF and store in it, d.p. = above 300 °C, yield: 5.785 g, 31 % based on final product, Anal. calc. For $C_{25}H_{42}N_5O_9Zn$: C, 48.27; H, 6.82; N, 11.26 found; C, 48.23; H, 6.78; N, 11.32 %. The XRD pattern of resulting product (Figure S2e) approved that compound **1** was synthesized successfully in large scale. The XRD pattern (Figure S2f) of this anionic MOF after exposure to air for three weeks indicates that although crystals of **1** lost its transparency in air, but it was stable and no destruction process was occurred for it.

Activation of $[HDMA]_2[Zn_2(BDC)_3(DMA)_2]$.6DMF (1) and preparation of its apohost material

The TGA diagram of **1** is different from that attributed to most of the reported MOFs and no apparent stage which attributed to removal of guest solvent molecules does not observed in its curve (Figure S4). The first and second stage of weight decrease in TGA curve attributed to removal of guest DMF molecules and probably to coordinated DMA. Where as the boiling point of DMF is about 153 °C and existence of these guest molecules in channels of this MOF up to high temperature of 320 °C is unreasonable. Since the TGA diagram of **1** did not give any information about finding removal temperature of guest DMF molecules, the suitable procedure for removal of them were finding by try and error technique. Initially as the boiling point of DMF is about 153 °C, a sample of **1** was putting in furnace at 153 °C for 8 hours. XRD pattern of this sample (Figure S6b) is similar to initially crystalline sample (Figure S6a) and approved that the crystalline structure of **1** was not change, but ^{1}H-NMR spectrum of this sample (Figure S7a) approved existence of some guest DMF molecules in channels of **1**. Then we put a sample of **1** in furnace at 320 °C for 8 hours. XRD pattern of this sample (Figure S6c) showed some changes in comparison with primary crystalline sample (Figure S6a) and the peak at $2\theta = 5.33°$ was disappeared and some changes were observed in other peaks, specially in $2\theta = 10°$ region. Probably activation at this temperature resulted in removal of coordinated DMA molecule and the structure of **1** was changed. Then we examined the exchange of guest DMF molecules with $CHCl_3$ and a sample of **1** statically was immersed in CHCl3 for 8 days. We expected that by this procedure the guest DMF molecules with high boiling point exchanges with $CHCl_3$ with low boiling point of 61 °C. ^{1}H-NMR spectrum of it (Figure S7b) showed the existence of both DMF and $CHCl_3$ molecules in compound **1** channels with the ratio of 1:1. Figure S6d shows the XRD pattern of this sample after heating at 90 °C for 8 hours in vacuum oven which approved the crystalline structure of **1** was not change but the ^{1}H-NMR spectrum (Figure S7c) of heated sample still shows the existence of DMF molecules in channels of **1**. Finally we exchanged guest DMF molecules with MeCN successfully. Selection of MeCN is due to linear structure of it and probably its easy removal from blocked channels of **1**. This guest exchange was done by immersing a sample of **1** in MeCN for 10 days, as the MeCN was

refreshed each day. XRD pattern (Figure S6e) and ^{1}H-NMR spectrum (Figure S7d) of this sample approve maintenance of initial crystalline structure and completely exchange of guest DMF molecules with MeCN, respectively. The peaks at 2.0 and 2.45 ppm in Figure S7d relate to methyl group of MeCN and $HDMA^{+}$ cation, respectively. Interstingly in **1** with MeCN guest molecules, unlike **1** with DMF gust molecules, removal of $HDMA^{+}$ cation occures without adding any excess amount of ammonium acatate. Since the boiling point of MeCN is about 81 °C, the exchanged sample with MeCN was heated in furnace at 100 °C for 8 hours. XRD pattern (Figure S6f) and ^{1}H-NMR spectrum (Figure S7e) of the activated sample approve maintenance of initial crystalline structure and completely removal of guest MeCN molecules, respectively. Thus the appropriate procedure for activation of this MOF was discovered.

Thermogravimetric analysis of $[HDMA]_2[Zn_2(BDC)_3(DMA)_2].6DMF$ (1)

Thermo gravimetric (TG) curve of **1** single crystal (Figure S4) shows mass loss of 80.0% in three steps between 160-500 °C. Mass loss calculations show that 41.0% (calcd 42.44%) of weight loss in first and second steps between 160-320 °C could be related to removal of six guest DMF molecules and two coordinated DMA species. XRD pattern (Figure S6c) of a compound **1** sample which was heated at 320 °C approved that removal of guest DMF molecules overlaps with structural destruction and removal of coordinated DMA molecules. Thus no distinct stage which attributes to formation of apohost framework, after DMF removal does not exist in **1**. In the next step weight loss of 39.0% between 320-500 °C could be related to removal of 3 BDC^{2-} and 2 $HDMA^{+}$ species accompanied with an exothermic effect at 500 °C. Finally 20.0% residue at 500 °C could be attributed to formation ZnO from thermlyses of **1**.

Postsynthetic cation exchange process of 1 with Ni^{2+}, Cu^{2+}, Li^{+}, Na^{+} and K^{+} ions

In order to studies these cation exchange process in a crystal to crystal transformation, initially we examined the stability of compound **1** crystallinity in various solvents such as methanol, ethanol, acetone, distilled water, acetonitrile, tetrahydrofuran (THF) and N,N′-dimethylformamide (DMF), but this MOF only retained its crystallinity in DMF. Thus

crystals of as-synthesized **1** were immersed in a saturated solution of $Ni(NO_3)_2$, $Cu(NO_3)_2,3H_2O$, $LiNO_3$, $NaNO_3$ and KI in DMF at room temperature. The crystals were soaked for ten days, during which time the saturated solution was refreshed three times daily. Unfortunately the crystallinity of these samples was not maintained during these cation exchange processes and we could not determine the structures of these cation exchanged samples by single crystal X-ray crystallography. After decanting the metal ion saturated solutions, the cation-exchanged samples were rinsed and soaked in DMF for up to three days to remove residual $Ni(NO_3)_2$, $Cu(NO_3)_2,3H_2O$, $LiNO_3$, $NaNO_3$ and KI from the frameworks. The results of ICP and elemental analysis for these five samples are summarized in Tables S1 and S2, respectively. Figures S8 and S12 shows the IR spectra of **2**,**3** and **4**-**6** MOF materials, respectively. In the case of performing cation exchange process with K^+ ion, we could not prepare saturated solution of KNO_3, KCl or K_2SO_4, because solubility of them is very low, thus we used KI with appropriate solubility in DMF.

Cation exchange of $HDMA^+$ with Ni^{2+} and Cu^{2+} ions

a) Why we selected these two metal ions for cation exchange process?

d^8 electronic configuration of Ni^{2+} usually result in formation of four coordinate square planner complexes. As some ligands like CO or CN^- cause in higher energy for one of the d orbitals ($3d_{x^2-y^2}$), finally 8 electrons of Ni^{2+} occupy other four d orbitals with lower energy stage. Thus $3d_{x^2-y^2}$, 4s, $4p_x$ and $4p_y$ orbitals common in formation of four dsp^2 orbitals. Nevertheless some tetrahedral complexes of Ni^{2+} were also reported which have little distortion and Td structure transformed to D_2d point group. In summary, the reason of selection Ni^{2+} for ion exchange is the opportunity of formation both square planner and tetrahedral structures by coordination number of four and octahedral structure with coordination number of six. Cu^{2+} ion with d^9 electronic configuration also could create square planner, tetrahedral and octahedral structures in its coordination sphere. Although in Cu^{2+}, similar to Ni^{2+}, square planner and octahedral structures are more common than tetrahedral structure. It should be also mentioned that Cu^{2+} complexes due to $[Ar]d^9$ electronic configuration in tetrahedral and especially in octahedral crystal fields shows Jahn & Teller distortion.

Now we have 3 opportunities in cation exchange process of **1** with these two metal ions:

1. Cation exchange only occurs with organic $HDMA^+$ cation.
2. Cation exchange only occurs with Zn^{2+} ion.
3. Both of Zn^{2+} ion and organic $HDMA^+$ cation common in cation exchange processes.

b) Cation exchange process of **1** with Ni^{2+}.

IR spectrum of **2** is illustrated in Figure S8a which does not have any significant difference to **1** (Figure S1c). Figure S9b shows the XRD pattern of compound **1** after cation exchange process in saturated solution of Ni^{2+}. The resulting pattern is similar to that of **1** (Figure S9a) which approved that the crystalline structure of exchanged sample (**2**) is identical to **1**. No change in XRD pattern of **2** in comparison with that of **1** indicates that probably cation exchange process of Ni^{2+} was not occurred with Zn^{2+}, because Zn^{2+} in **1** have Td structure but Ni^{2+} with coordination number of four and six usually forms square planner and octahedral structure. If this cation exchange process was occurred, the XRD pattern of exchanged sample would be changed.

Figure S10a shows the ^{1}H-NMR spectrum of compound **1** crystalline sample after several wash with acetone in order to removal of surface adsorbed DMF molecules. Since this MOF due to its especial 3D framework is in soluble, d_6-DMSO molecules solvent exchange with guest DMF molecules results in appearance of DMF peaks at 2.71 and 2.87 ppm. Figure S10b attributes to crystalline sample of **1** in the presence of excess ammonium acetate. Existence of excess ammonium (NH_4^+) ions in NMR tube, results in replacement of $HDMA^+$ with NH_4^+ ions. Thus $HDMA^+$ organic cations removed from channels of **1** and enter to solution phase. Now $HDMA^+$ peak could be observed at 2.45 ppm. The observed peak in region of 1.74-1.80 ppm attributed to existance of excess acetate (CH_3COO^-) ions in solution. Figure S10c shows the ^{1}H-NMR spectrum of **2** after several wash with acetone. As the $HDMA^+$ peak only appear in existance of excess ammonium acetate, we added 5mg of $NH_4^+COO^-$ to the NMR tube of **2**. Figure S10c shows that $HDMA^+$ peak at 2.45 ppm was disappear which indicates that completely replacement of $HDMA^+$ ions were occured by Ni^{2+} ions.

ICP results (Table S1) show the existance of 9.16 and 17.82 ppm of Ni^{2+} and Zn^{2+} in 25 ml solution of **2**. Thus the molar ratio of Ni^{2+}:Zn^{2+} is equal to 1.14:2. By consideration of compound **1** molecular formula ($[HDMA]_2[Zn_2(BDC)_3(DMA)_2].6DMF$) and with attention to +2 valence of Ni ion, if $HDMA^+$ was replaced with Ni^{2+}, the expected molar ratio of Ni^{2+}:Zn^{2+} would be obtained as 1:2. The observed value from the ICP analyses with respect to measurement inaccuracy is correct. Finally with attention to no significant change in XRD pattern of **2** (Figure S9b) in comparison with initial sample of **1** (Figure S9a), we could conclude that in this cation exchange process only replacement of $HDMA^+$ with Ni^{2+} was occured and Zn^{2+} metal ions were not exchanged.

The results obtaied from elemental analyses of **2** and that calculated for this new MOF could be observed in Table S2. We spoted probability of existance various numbers of guest DMF molecules in channels of **1**. Really replacement of two organic cation of $HDMA^+$ with one Ni^{2+} ion, creates a hollow sphere in channels of this MOF which probablly occupied with one DMF molecule from the solvent applied for cation exchange process.

Figure S11a shows the TGA diagram of **2**. The observed mass loss of 39.0% (calcd 39.9%) in first stage of this curve is approximately near to that observed in **1** (Figure S4), which approved the existence of 7 DMF molecules in channels of **2**. On the other hand, formation of 29.7% (calcd 28.2%) residue from **2** at 580 °C is 9.7% higher than that observed in **1** which with attention to replacement of two organic cation of $HDMA^+$ with one Ni^{2+} ion and prospect of formation 2.0 ZnO + 1.0 NiO by temperature increase to 600 °C could be explained.

Finally with respect to the obtained results from XRD pattern, ^{1}H-NMR spectrum, ICP, CHN and TGA analyses, we could propose $Ni[Zn_2(BDC)_3(DMA)_2].7DMF$ molecular formula for MOF of **2**.

c) Cation exchange process of **1** with Cu^{2+}.

IR spectrum of **3** is illustrated in Figure S8b which is approximately different from that observed in **1**, especially in their fingerprint region (Figure S1c). Figure S9d shows the XRD pattern of compound **1** after cation exchange process in saturated solution of Cu^{2+}. As it is obvious, the resulting pattern does not match with XRD pattern of **1** (Figure S9a)

which approved that the crystalline structure of exchanged sample (**3**) is different from **1**. As was mentioned previously, Cu^{2+} ion leans to forms square planner (with C.N. = 4) or distorted octahedral structure (with C.N. = 6). Coordination behaviour of carboxylate ligands around Zn^{2+} ion in **1** (Figure S3a) shows the opportunity of formation these two structures for Cu^{2+} ion. Change in XRD pattern of **3** in comparison with that of **1** encourages the probability of Zn^{2+} cation exchange reaction with Cu^{2+}.

Figure S10d shows the ^{1}H-NMR spectrum of **3** after several wash with acetone in the presence of 5mg ammonium acetate. Disappearance of $HDMA^{+}$ peak at 2.45 ppm indicates that replacement of $HDMA^{+}$ ions with Cu^{2+} ions occured completely.

ICP results (Table S1) show the existance of 32.08 and 1.82 ppm of Cu^{2+} and Zn^{2+} in 25 ml solution of **3**. Thus the molar ratio of Cu^{2+}:Zn^{2+} is equal to 36.06:2. By consideration of compound **1** molecular formula ($[HDMA]_2[Zn_2(BDC)_3(DMA)_2].6DMF$) and with attention to +2 valence of Cu ion, if $HDMA^{+}$ was only replaced with Cu^{2+}, the expected molar ratio of Cu^{2+}:Zn^{2+} would be obtained as 1:2. But the observed molar ratio is 36 orders higher than that expected when the cation exchange reaction only occurs with $HDMA^{+}$. Finally with attention to change in XRD pattern of **3** (Figure S9d) in comparison with initial sample of **1** (Figure S9a) and also disappearance of $HDMA^{+}$ peak in ^{1}H-NMR spectrum of **3**, we could conclude that in this cation exchange process both of Zn^{2+} ions and organic $HDMA^{+}$ cations replaced with Cu^{2+}.

The results observed from elemental analyses of **3** and that calculated for existance or absence of coordinated DMA molecule to Zn^{2+} and various guest solvent molecules in channels of this new MOF could be observed in Table S2. A comparison between ٪N of **3** with metal-organic framework of **1**, indicates that ٪N was 43٪ decreased. In addition to disapearance of $HDMA^{+}$ peak at 2.45 ppm in ^{1}H-NMR spectrum of **3**, CHN analyses results approved the replacement of organic cation with Cu^{2+}. Extreme decrease of ٪N could shows that probably some of guest DMF molecules were eleminate from channels or pores of **3**. Another attention to Figure S3a shows that there are three mono coordinated carboxylate group and one DMA molecule in tetrahedral coordination sphere of Zn^{2+}. If Zn^{2+} ion is exchanged with Cu^{2+}, it mays that three mono coordinated carboxylate groups chelate to Cu^{2+} ion, DMA removes from Cu^{2+} coordination sphere and Cu^{2+} with distorted octahedral structure forms. The observed and calculated values

for CHN analyses of **3** indicate that we could propose two molecular formula for **3**, $Cu[Cu_2(BDC)_3(DMA)_2].2DMF$ and $Cu[Cu_2(BDC)_3].4DMF$, but the observed value is more similar to $Cu[Cu_2(BDC)_3].4DMF$ than $Cu[Cu_2(BDC)_3(DMA)_2].2DMF$.

Figure S11b shows the TGA diagram of **3**. The observed mass loss of 27.0% (calcd 30.0%) in first stage of this curve between the temperature range of 108 to 350 °C is probably due to removal of guest DMF molecules. On the other hand, formation of 40.0% (calcd 37.4%) residue from **3** with respect to replacement of both Zn^{2+} and $HDMA^+$ cations with Cu^{2+} ion and prospect of formation 3.0 CuO by temperature increase up to 500 °C could be explained.

Finally with respect to the obtained results from XRD pattern, ^{1}H-NMR spectrum, ICP, CHN and TGA analyses, we could propose $Cu[Cu_2(BDC)_3].4DMF$ molecular formula for MOF of **3**.

Cation exchange of $HDMA^+$ with Li^+, Na^+ and K^+ ions

a) Cation exchange process of **1** with Li^+.

IR spectrum of **4** is illustrated in Figure S12a which does not have any significant difference to **1** (Figure S1c). Figure S13b shows the XRD pattern of compound **1** after cation exchange process in saturated solution of Li^+. As it is obvious, the resulting pattern approximately matches with XRD pattern of **1** (Figure S13a), but the initial peak at $2\theta = 5.33°$ shifts to $2\theta = 6.93°$ which approved that the attributed space between the two crystalline plate becomes shorter than that in **1**. This phenomenon results in formation of narrower channels with less guest DMF molecules in comparison with **1** which approved by CHN and TG analyses, too. XRD pattern likeness of **4** to that of **1** indicates that cation exchange process of Li^+ occurred with $HDMA^+$.

Figure S14b shows the ^{1}H-NMR spectrum of **4** after several wash with acetone in the presence of 5mg ammonium acetate. Disappearance of $HDMA^+$ peak at 2.45 ppm indicates that replacement of $HDMA^+$ ions with Li^+ ions occured completely.

ICP results (Table S1) show the existance of 0.49 and 49.75 ppm of Li^+ and Zn^{2+} in 25 ml solution of **4**. Thus the molar ratio of Li^+:Zn^{2+} is equal to 0.94:1. By consideration of compound **1** molecular formula ($[HDMA]_2[Zn_2(BDC)_3(DMA)_2].6DMF$) and with attention to +1 valence of Li ion, if $HDMA^+$ was replaced with Li^+, the expected molar

ratio of Li^+:Zn^{2+} would be obtained as 1:1. The observed value from the ICP analyses with respect to measurement inaccuracy is correct. Finally with attention to no apparent change in XRD pattern of **4** (Figure S13b) in comparison with initial sample of **1** (Figure S13a), we could conclude that in this cation exchange process, replacement of $HDMA^+$ with Li^+ was occured succesfully.

The results obtaied from elemental analyses of **4** and that calculated for this new MOF could be observed in Table S2. We spoted probability of existance various numbers of guest DMF molecules in channels of **4**. The calculated values for $Li_2[Zn_2(BDC)_3(DMA)_2].4DMF$ matches with those observed for **4**. Shift of the initial peak at $2\theta = 5.33°$ to $2\theta = 6.93°$ which approved that the attributed space between the two crystalline plate becomes shorter in **4** in comparison with **1** also indicates that vacant sphere of channels in **4** become smaller and thus decrease of guest DMF molecules from six in **1** to four in **4** could be explained.

Figure S15a shows the TGA diagram of **4**. The observed mass loss of 29.5% (calcd 28.68%) in first stage of this curve up to 340 °C is due to removal of guest DMF molecules. On the other hand, formation of 29.0% (calcd 28.84%) residue from **4** at 602 °C which is 9.0% higher than that observed in **1** with respect to formation 2.0 ZnO + 1.0 Li_2O by temperature increase up to 602 °C could be explained.

Finally with respect to the obtained results from XRD pattern, ^{1}H-NMR spectrum, ICP, CHN and TGA analyses, we could propose $Li_2[Zn_2(BDC)_3(DMA)_2].4DMF$ molecular formula for MOF of **4**.

b) Cation exchange process of **1** with Na^+.

IR spectrum of **5** is illustrated in Figure S12b which does not have any significant difference to **1** (Figure S1c). Figure S13d shows the XRD pattern of compound **1** after cation exchange process in saturated solution of Na^+. The resulting pattern is similar to that of **1** (Figure S13a), which approved that crystalline structure of **5** is wholly similar to **1** and cation exchange process of Na^+ occurred with $HDMA^+$, too.

Figure S14c shows the ^{1}H-NMR spectrum of **5** after several wash with acetone in the presence of 5mg ammonium acetate. Disappearance of $HDMA^+$ peak at 2.45 ppm indicates that replacement of $HDMA^+$ ions with Na^+ ions occured completely.

ICP results (Table S1) show the existance of 0.733 and 1.93 ppm of Na^+ and Zn^{2+} in 25 ml solution of **5**. Thus the molar ratio of Na^+:Zn^{2+} is equal to 1.08:1. By consideration of compound **1** molecular formula ($[HDMA]_2[Zn_2(BDC)_3(DMA)_2].6DMF$) and with attention to +1 valence of Na ion, if $HDMA^+$ was replaced with Na^+, the expected molar ratio of Na^+:Zn^{2+} would be obtained as 1:1. The observed value from the ICP analyses with respect to measurement inaccuracy is correct. Finally with attention to no apparent change in XRD pattern of **5** (Figure S13d) in comparison with initial sample of **1** (Figure S13a), we could conclude that in this cation exchange process, replacement of $HDMA^+$ with Na^+ was occured succesfully.

The results obtaied from elemental analyses of **5** and that calculated for this new MOF could be observed in Table S2. We spoted probability of existance various numbers of guest DMF molecules in channels of **5**. The calculated values for $Na_2[Zn_2(BDC)_3(DMA)_2].6DMF$ matches with those observed for **5**.

Figure S15b shows the TGA diagram of **5**. The observed mass loss of 34.68% (calcd 36.62%) in first stage of this curve up to 310 °C is due to removal of guest DMF molecules. On the other hand, formation of 27.82% (calcd 28.64%) residue from **5** at 495 °C which is 7.82% higher than that observed in **1** with respect to formation 2.0 ZnO + 1.0 Na_2O by temperature increase up to 495 °C could be explained.

Finally with respect to the obtained results from XRD pattern, ^{1}H-NMR spectrum, ICP, CHN and TGA analyses, we could propose $Na_2[Zn_2(BDC)_3(DMA)_2].6DMF$ molecular formula for MOF of **5**.

c) Cation exchange process of **1** with K^+.

IR spectrum of **6** is illustrated in Figure S12c which shows some differences in comparison with that observed in **1** (Figure S1c). Figure S13f shows the XRD pattern of compound **1** after cation exchange process in saturated solution of K^+. As it is obvious, the resulting pattern is completely different from XRD pattern of **1** (Figure S13a), which approved that crystalline structure of **6** is wholly different from **1**. Our search also shows the existence of KI in crystalline structure of **6**. The characteristic peaks of KI in Figure S13f matches with the cubic pattern of it with the lattice parameters of a = 7.0655 Å and z = 4 (JCPDS card number 04-0471).

Figure S14c shows the ^{1}H-NMR spectrum of **6** after several wash with acetone in the presence of 5mg ammonium acetate. Appearance of DMF peaks in ^{1}H-NMR spectrum of **6** indictes that it is a porous MOF material. Disappearance of $HDMA^+$ peak at 2.45 ppm indicates that replacement of $HDMA^+$ ions with K^+ ions occured completely.

ICP results (Table S1) show the existance of 8.02 and 0.321 ppm of K^+ and Zn^{2+} in 25 ml solution of **6**. Thus the molar ratio of K^+:Zn^{2+} is equal to 40.9:1. By consideration of compound **1** molecular formula ($[HDMA^+]_2[Zn_2(BDC)_3(DMA)_2]^{2-}$.6DMF) and with attention to +1 valence of K ion, if $HDMA^+$ was replaced with K^+, the expected molar ratio of K^+:Zn^{2+} would be obtained as 1:1. The observed value from the ICP analyses is 41 orders higher that that expected, which with respect to results of XRD pattern and ^{1}H-NMR spectrum, we could conclude that in addition to completely exchange of $HDMA^+$ with K^+, probably the pores of **6** were occupied with precipitated KI from its saturated solution.

The results obtaied from elemental analyses of **6** could be observed in Table S2, but due to structural change of **6** in comparison with **1** and existance of excess KI in the pores of this new material, we are unable to proposed any molecular formula for it.

Figure S15c shows the TGA diagram of **6**. The observed mass loss of 6.15% in first stage of this curve up to 380 °C is due to removal of guest DMF molecules. On the other hand, formation of 56.64% residue from **6** at 691 °C which is 36.64% higher than that observed in **1** related to formation a mixture of ZnO and KI by temperature increase up to 691 °C.

Activation of cation exchanged samples and preparation of their apohost material

Preparation apohost frameworks of cation exchanged samples with Ni^{2+}, Cu^{2+}, Li^+, Na^+ and K^+ ions were done by similar procedure to that applied for **1**. Exchange of guest DMF solvent molecules were done by immersing a sample of each **2**-**6** materials in MeCN for 10 days, as the MeCN was refreshed daily. Since the boiling point of MeCN is about 81 °C, the exchanged sample with MeCN was heated in furnace at 100 °C for 8 hours. XRD patterns of activated samples (Figures S9c,e and S13c,e,g for **2**,**3** and **4**-**6**, respectively) approve maintenance of initial crystalline structure, except for **4**, it seems that this MOF has flexible dynamic structure as by removal of guest MeCN molecules from its channels the two peaks at $2\theta = 6.93$ and 9.73° shift to each other and appear at 2θ

= 7.29 and 8.81°. These changes in position of XRD pattern peaks probably attributed to changes in pore diameter of its channels during the formation of apohost framework.

The relation between N_2 gas sorption capacities of 1-6 with van der Waals radius of metal ions

In **2** and **3** with Ni^{2+} and Cu^{2+} cation ions, N_2 gas sorption amounts of 34 and 67 cm^3(STP)/g at P/P_0 = 1.0 are compatible with van der Waals radius of 1.63 and 1.40 Å, respectively. Really with decrease of van der Waals radius from Ni^{2+} to Cu^{2+}, the resistance of channels for entrance of N_2 molecules is decreased and the amounts of N_2 gas sorption is increased. In **4**, as exhibited by XRD pattern (Figure S13c), prescence of Li^+ cations results in shift of two initial peaks at 2θ = 6.93 and 9.73° to 2θ = 7.33 and 8.81° which probably result in change of channel shapes with similar width and length. Thus by regardless to higher van der Waals radii of Li^+ (1.82 Å), apohost framework of **4** shows high N_2 gas sorption amount of 166 cm^3(STP)/g at P/P_0 = 1.0. In apohost framework of **5**, with similar structure to **1**, existance of Na^+ ion with van der Waals radii of 2.27 Å in rectangular channels results in low N_2 gas sorption amount of 24 cm^3(STP)/g at P/P_0 = 1.0. No enough information about structure and molecular formula of **6**, make us unable to explain N_2 gas sorption amount of 83 cm^3(STP)/g at P/P_0 = 1.0 for this compound.

XRD pattern identification of residues prepared from calcination process of 1-6

The XRD pattern of residue from calcination process of **1** (Figure S17a) is in agreement with the typical wurtzite structure of ZnO (hexagonal phase, space group $P6_3mc$, with lattice constants $a = 3.24982(9)$ Å, $c = 1.6021$ Å, $Z = 2$, JCPDS No. 36–1451). In MOF material of **2**, the XRD pattern of obtained residue (Figure S17b) matches with the above hexagonal phase of ZnO and $Ni_{0.9}Zn_{0.1}O$ (cubic phase, space group $Fm3m$, with lattice constants $a = 4.188(4)$ Å, $Z = 4$, JCPDS No. 75–0270). The XRD pattern of residue from calcination process of **3** (Figure S17c) is in agreement with the typical tenorite structure of CuO (monoclinic phase, space group $C2/c$, with lattice constants $a = 4.6883(4)$ Å, $b = 3.4229(2)$ Å, $c = 5.1319(3)$ Å, $\beta = 99.506(4)$, $Z = 4$, JCPDS No. 48–1548). In the case of **4**, XRD pattern of obtained residue (Figure S17d) matches with the above hexagonal

phase of ZnO and Li_2O (cubic phase, space group *Fm3m*, with lattice constants *a = 4.6114* Å, *Z = 4*, JCPDS No. 12–0254). The XRD pattern of residue (Figure S17e) from calcination process of **5** is in agreement with the above wurtzite structure of ZnO and $Na_2CO_3 \cdot H_2O$ (orthorhombic phase, space group $P2_1ab$, with lattice constants *a = 6.472* Å, *b = 10.724* Å, *c = 5.259* Å, *Z = 4*, JCPDS No. 76–0910). Finally in **6**, the obtained XRD pattern (Figure S17f) from calcination of it matches with the above wurtzite structure of ZnO and $K_2CO_3 \cdot (H_2O)_{1.5}$ (monoclinic phase, space group *C2/c*, with lattice constants *a = 11.887(6)* Å, *b = 13.827(3)* Å, *c = 7.112(2)* Å, *β = 120.560(3)*, *Z = 8*, JCPDS No. 73–0470).

Table S1. Results of the ICP analyses obtained for MOF materials of **2-6**.

	Amount of M^{2+} or M^+ ion (g)	Amount of Zn^{2+} ion (g)	Amount of M^{2+} or M^+ ion (mol)	Amount of Zn^{2+} ion (mol)	The ratio of M^{2+}:Zn^{2+} or M^+:Zn^{2+}	The expected ratio in cation exchange with DMA^+
2 (M^{2+}:Ni^{2+})	9.16×10^{-3}	1.782×10^{-2}	3.90×10^{-6}	6.81×10^{-6}	1.14:2	1:2
3 (M^{2+}:Cu^{2+})	3.208×10^{-2}	1.82×10^{-3}	1.262×10^{-5}	7.00×10^{-7}	36.06:2	1:2
4 (M^+:Li^+)	4.943×10^{-4}	4.975×10^{-2}	1.781×10^{-5}	1.902×10^{-5}	0.94:1	1:1
5 (M^+:Na^+)	7.33×10^{-4}	1.93×10^{-3}	7.97×10^{-7}	7.34×10^{-7}	1.08:1	1:1
6 (M^+:K^+)	8.02×10^{-3}	3.21×10^{-4}	5.131×10^{-6}	1.23×10^{-7}	40.9:1	1:1

Table S2. Results of the elemental analyses obtained for MOF materials of **2**-**6**.

2	Obs	Cal for 2DMF	Cal for 4DMF	Cal for 6DMF	Cal for 7DMF	Cal for 8DMF	Cal for 10DMF
%C	45.79	44.48	45.14	45.64	45.85	46.03	46.35
%H	5.92	4.40	5.12	5.67	5.90	6.10	6.45
%N	9.88	6.10	7.90	9.26	9.82	10.33	11.19

		With	coordinated	DMA	molecule	Without	coordinated	DMA	molecule
3	Obs	Cal for 2DMF	Cal for 4DMF	Cal for 6DMF	Cal for 7DMF	Cal for 2DMF	Cal for 4DMF	Cal for 6DMF	Cal for 7DMF
%C	44.40	44.42	45.09	45.59	45.80	43.46	44.33	44.98	45.24
%H	4.10	4.39	5.12	5.67	5.89	3.17	4.14	4.86	5.16
%N	5.79	6.10	7.90	9.25	9.81	3.38	5.75	7.49	8.21

4	Obs	Cal for 2DMF	Cal for 4DMF	Cal for 6DMF	Cal for 8DMF
%C	47.20	46.76	47.12	47.39	47.60
%H	5.27	4.63	5.35	5.89	6.31
%N	8.31	6.42	8.24	9.61	10.68

5	Obs	Cal for 2DMF	Cal for 4DMF	Cal for 6DMF	Cal for 8DMF
%C	46.03	45.10	45.68	46.12	46.47
%H	5.73	4.46	5.13	5.68	6.16
%N	9.44	6.19	7.99	9.36	10.42

6	Obs
%C	42.40
%H	2.50
%N	0.73

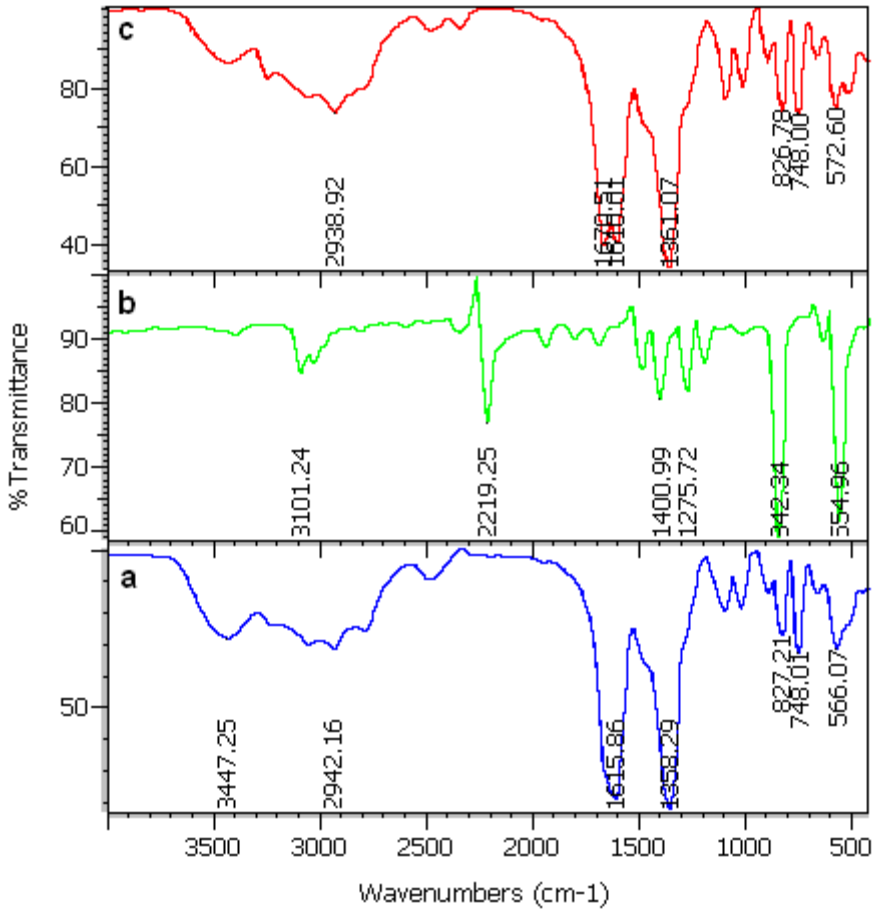

Figure S1. IR spectra of a) white powders of compound **1** prepared without addition of terephthalodinitrile, b) terephthalodinitrile and c) crystals of **1** suitable for single crystal X-ray analyses, obtained in the presence of terephthalodinitrile.

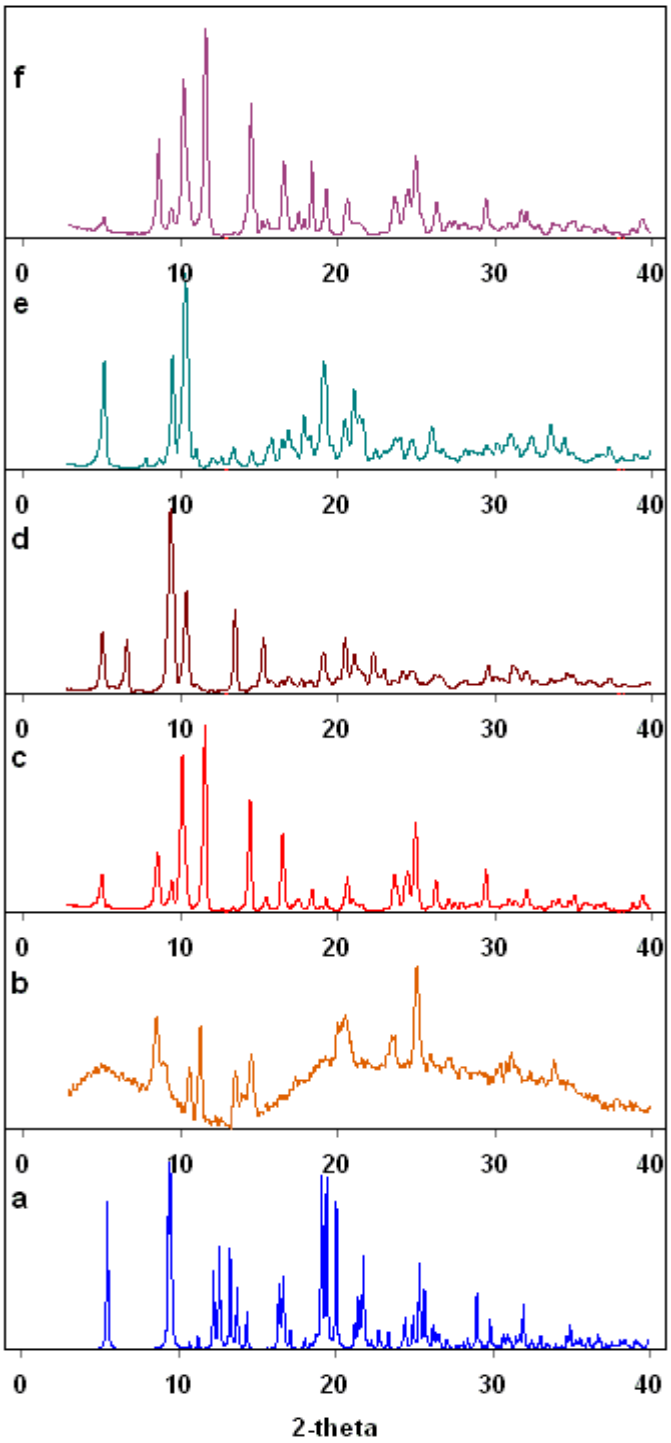

Figure S2. The XRD patterns of (a) simulated from single crystal X-ray data of compound **1**, (b) white powders of compound **1** prepared without addition of terephthalodinitrile, (c) crystals of **1** suitable for single crystal X-ray analyses, obtained in the presence of terephthalodinitrile, (d) white powders obtained under reflux condition, (e) crystals prepared in the large scale syntheses of compound **1** and (f) crystals of **1** after exposure to air atmosphere for 3 weeks.

Table S3. Crystal data and structure refinement for compound (**1**).

Empirical formula	$C_{25}H_{42}N_5O_9Zn$
Formula weight	622.01
Temperature	193(2) K
Wavelength	1.54187 Å
Crystal system	Monoclinic
Space group	P $2_1/c$
Unit cell dimensions	a = 17.546(3) Å
	b = 11.158(2) Å
	c = 18.392(3) Å
	$\alpha = 90.00^o$
	$\beta = 118.33(2)^o$
	$\gamma = 90.00^o$
Volume	3169.5(11) $Å^3$
Z	4
Density (calculated)	1.304 $g.cm^{-3}$
Absorption coefficient	1.535 mm^{-1}
F(000)	1316
Crystal size	0.53 × 0.19 × 0.12 mm^3
Theta range for data collection	2.86 to 66.98^o
Index ranges	$-20 \leq h \leq 20$
	$-7 \leq k \leq 13$
	$-21 \leq l \leq 18$
Reflections collected	12440
Independent reflections	5351 [R(int) = 0.0693]
Absorption correction	Semi-empirical from equivalents
Max. and min. transmission	1.000 and 0.695
Refinement method	Full-matrix least-squares on F^2
Data / restraints / parameters	5344 / 0 / 377
Goodness-of-fit on F^2	1.150
Final *R* indices [I>2σ (*I*)]	R_1= 0.0619
	wR_2= 0.1491
R Indices (all data)	R_1= 0.0798
	wR_2= 0.1810
Largest diff. Peak, hole	0.753 and -0.679 e.$Å^{-3}$

Table S4. Selected bond lengths /Å and angles /° for compound (**1**).

Zn(1)-O(1)	1.909(3)	O(1)-Zn(1)-O(3)	85.89(12)
Zn(1)-O(3)	1.979(3)	O(1)-Zn(1)-N(1)	113.72(15)
Zn(1)-N(1)	2.045(4)	O(3)-Zn(1)-N(1)	111.25(17)
Zn(1)-O(5)	2.053(3)	O(1)-Zn(1)-O(5)	125.24(12)
		O(3)-Zn(1)-O(5)	117.42(12)
		N(1)-Zn(1)-O(5)	102.95(14)

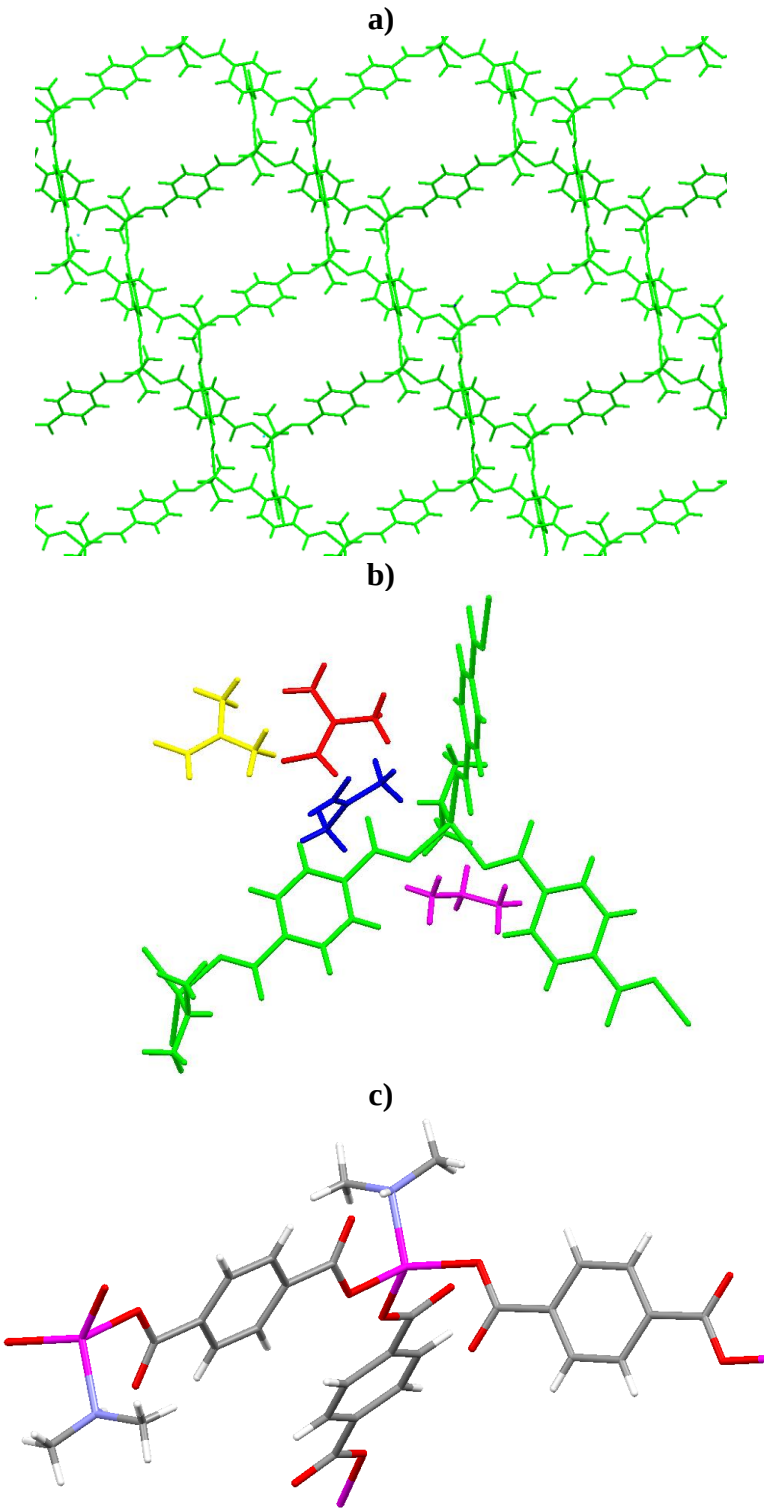

Figure S3. Showing the a) structure of one-dimensional channels in **1**, b) structure of the basic polymeric building block of compound **1** with three DMF molecules (red, blue and yellow species) and DMA^{+} organic cation (violet species) and c) coordination sphere around Zn^{II} ion in **1** (Zn = violet, O = red, N = blue, C = gray and H = white).

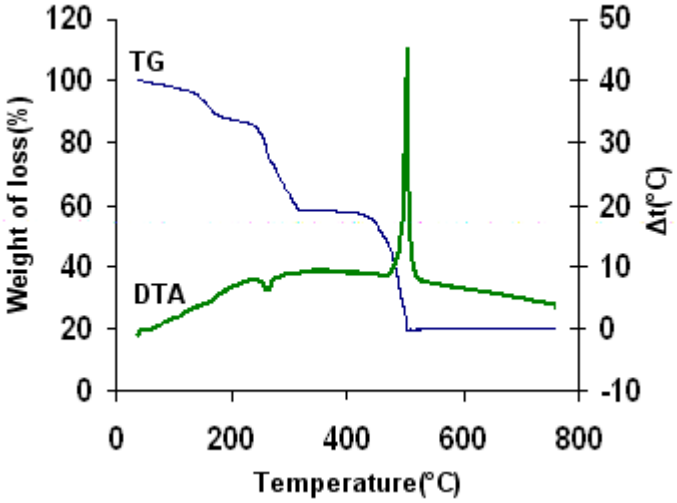

Figure S4. TG-DTA diagram of compound **1** single crystal in a static atmosphere of nitrogen.

Figure S5. Showing the pictures from MOF materials of **1** (a), **2** (b), **3** (c), **4** (d), **5** (e) and **6** (f).

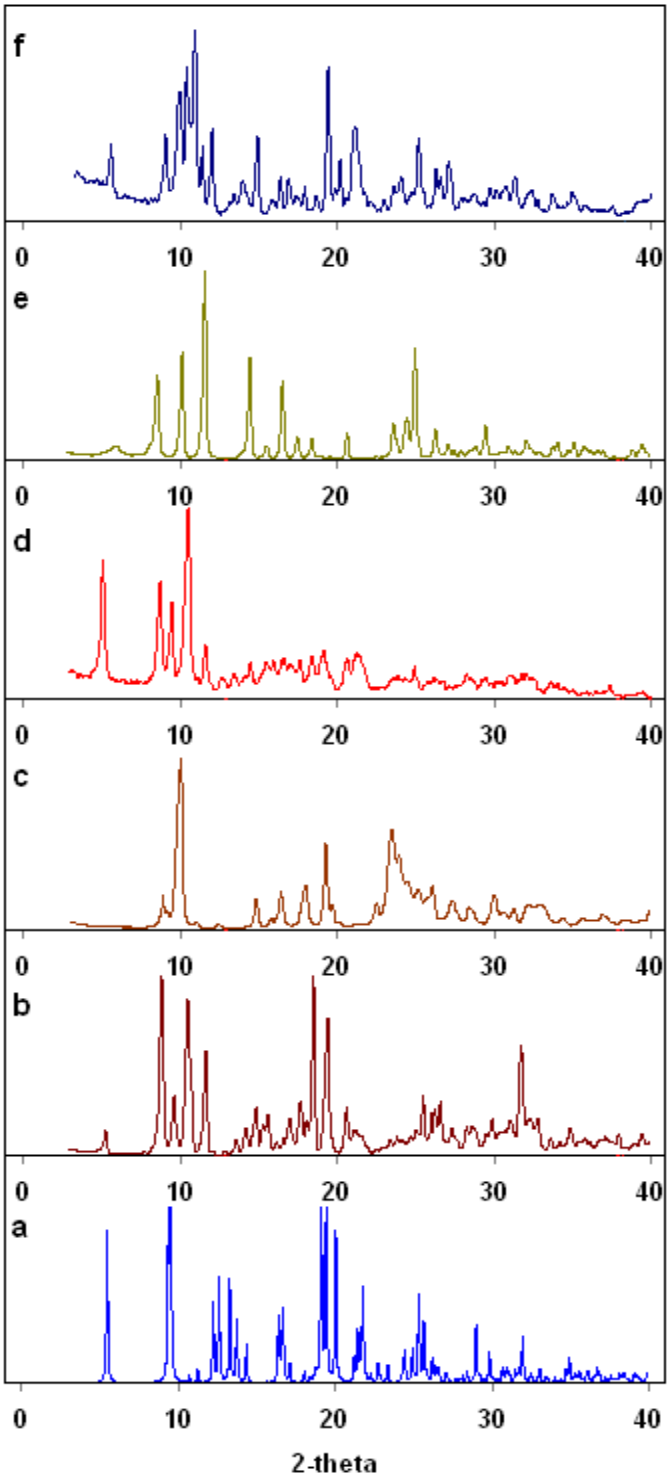

Figure S6. The XRD patterns of (a) simulated from single crystal X-ray data of compound **1**, (b) the sample obtained after heating **1** at 150 °C for 8 hours, (c) the sample obtained after heating **1** at 320 °C for 8 hours, (d) the sample obtained after heating **1** at 80 °C for 8 hours in vacuum oven after DMF exchange with $CHCl_3$, (e) **1** after solvent exchange with MeCN and (f) the sample obtained after heating **1** at 100 °C for 8 hours after DMF exchange with MeCN.

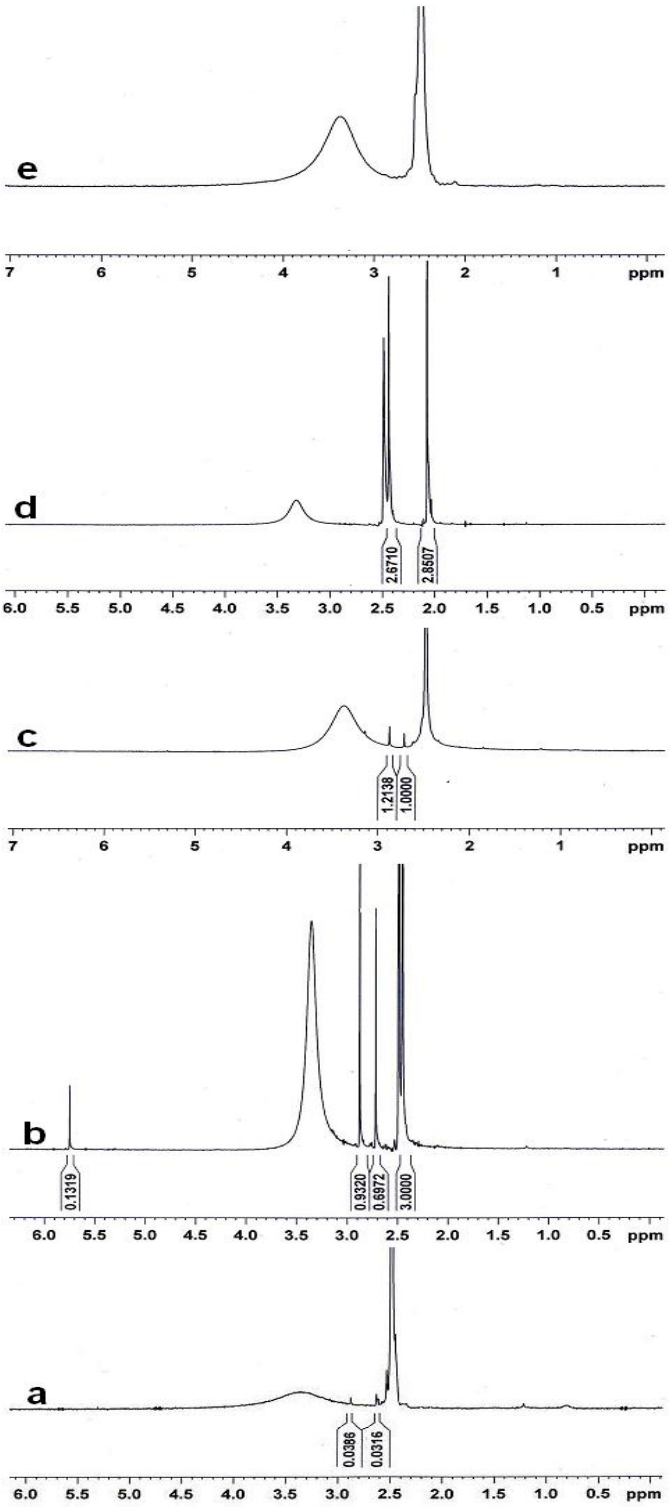

Figure S7. The ^{1}H-NMR spectra of (a) the sample obtained after heating **1** at 150 °C for 8 hours, (b) the sample obtained after DMF exchange with $CHCl_3$, (c) the sample obtained after heating **1** at 80 °C for 8 hours after DMF exchange with $CHCl_3$, (d) **1** after solvent exchange with MeCN and (e) the sample obtained after heating **1** at 100 °C for 8 hours after DMF exchange with MeCN.

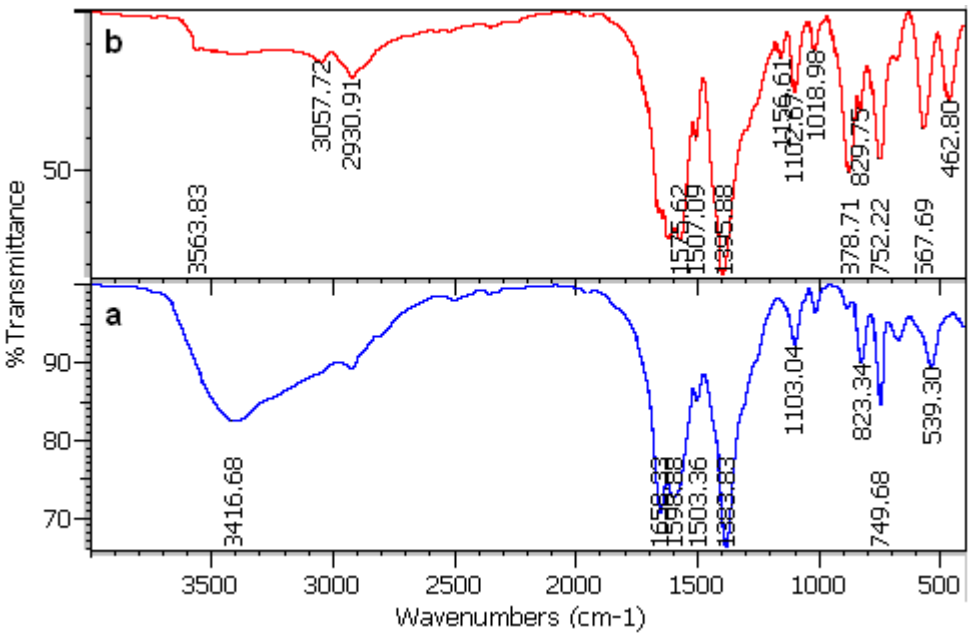

Figure S8. IR spectra of a) **2** and b) **3** MOF materials.

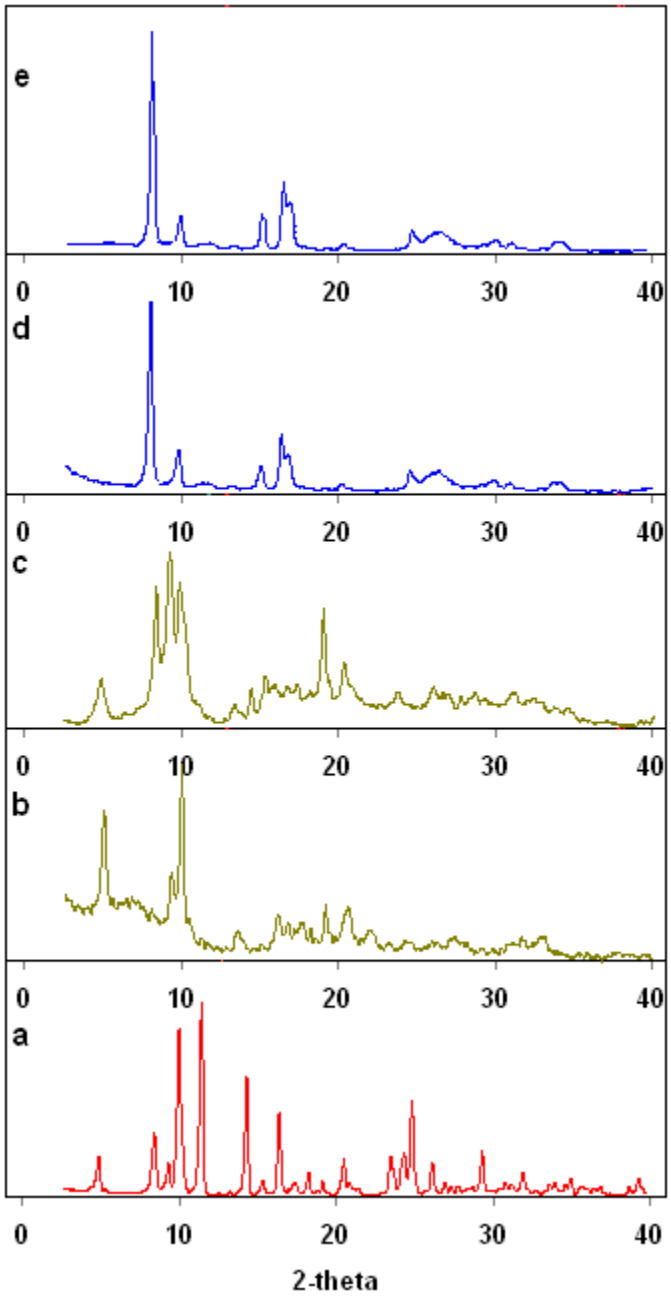

Figure S9. The XRD patterns of (a) compound **1** crystals, (b) compound **2** obtained after cation exchange with Ni^{2+}, (c) compound **2** after activation at 100 °C for 8 hours, (d) compound **3** obtained after cation exchange with Cu^{2+} and (e) compound **3** after activation at 100 °C for 8 hours.

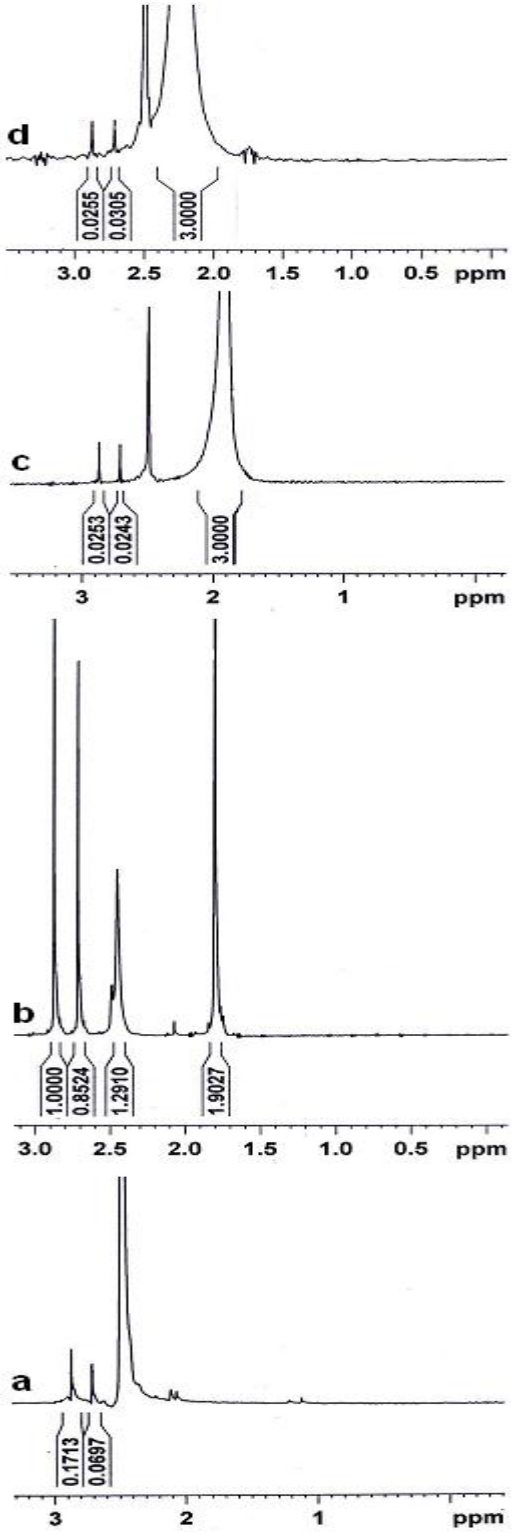

Figure S10. The ^{1}H-NMR spectra of (a) compound **1**, (b) compound **1** after addition of 5 mg ammonium acetate to the tube, (c) compound **2** after addition of 5 mg ammonium acetate to the tube and (d) compound **3** after addition of 5 mg ammonium acetate to the tube.

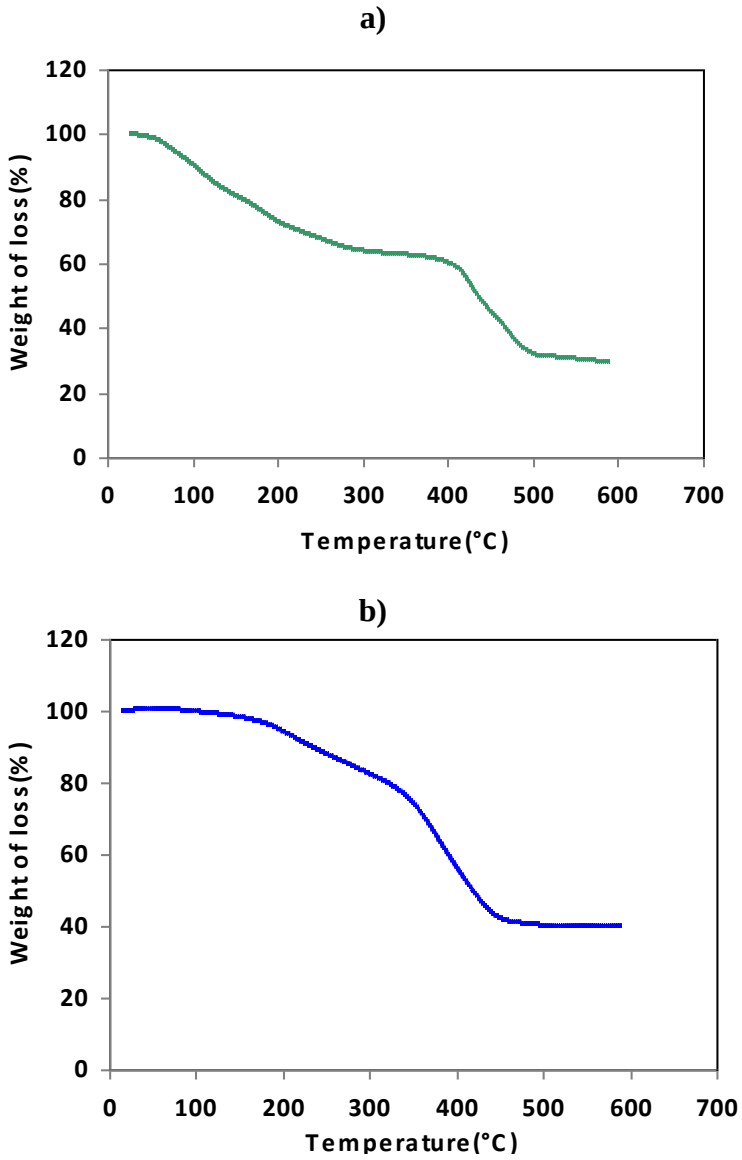

Figure S11. TGA curves of **2** (a) and **3** (b) MOF materials in a static atmosphere of nitrogen.

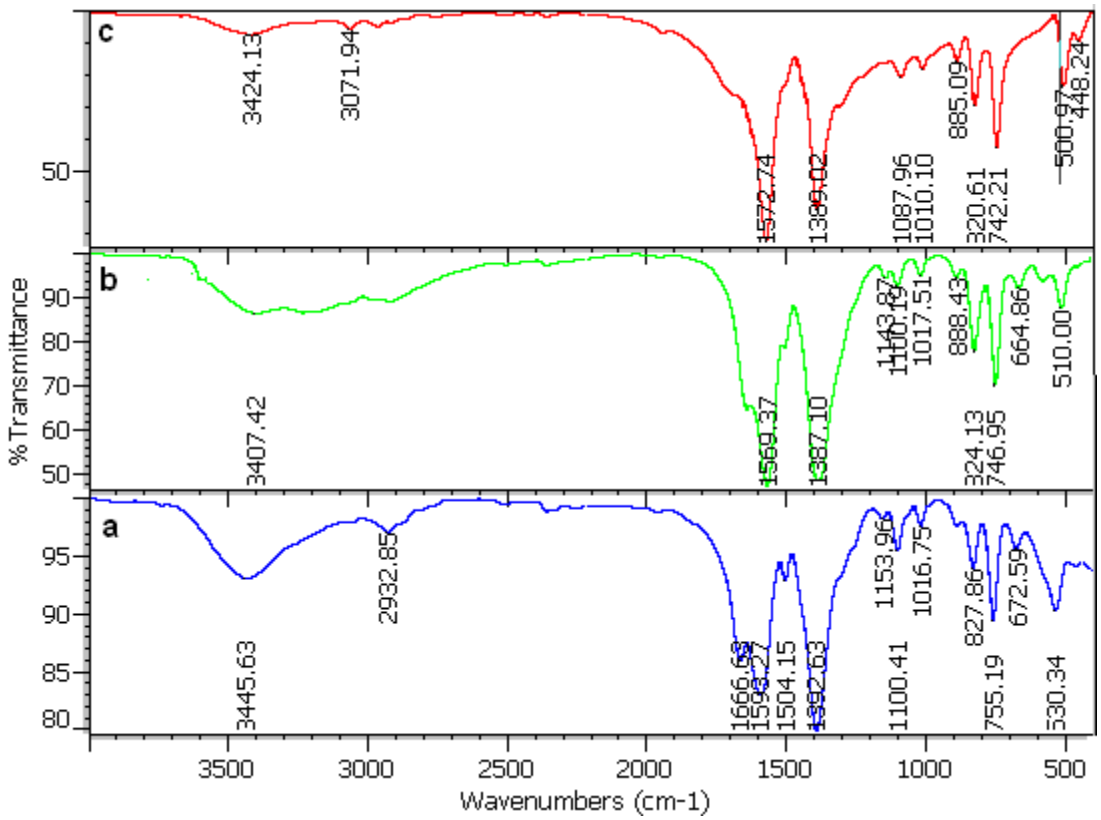

Figure S12. IR spectra of a) **4**, b) **5** and c) **6** MOF materials.

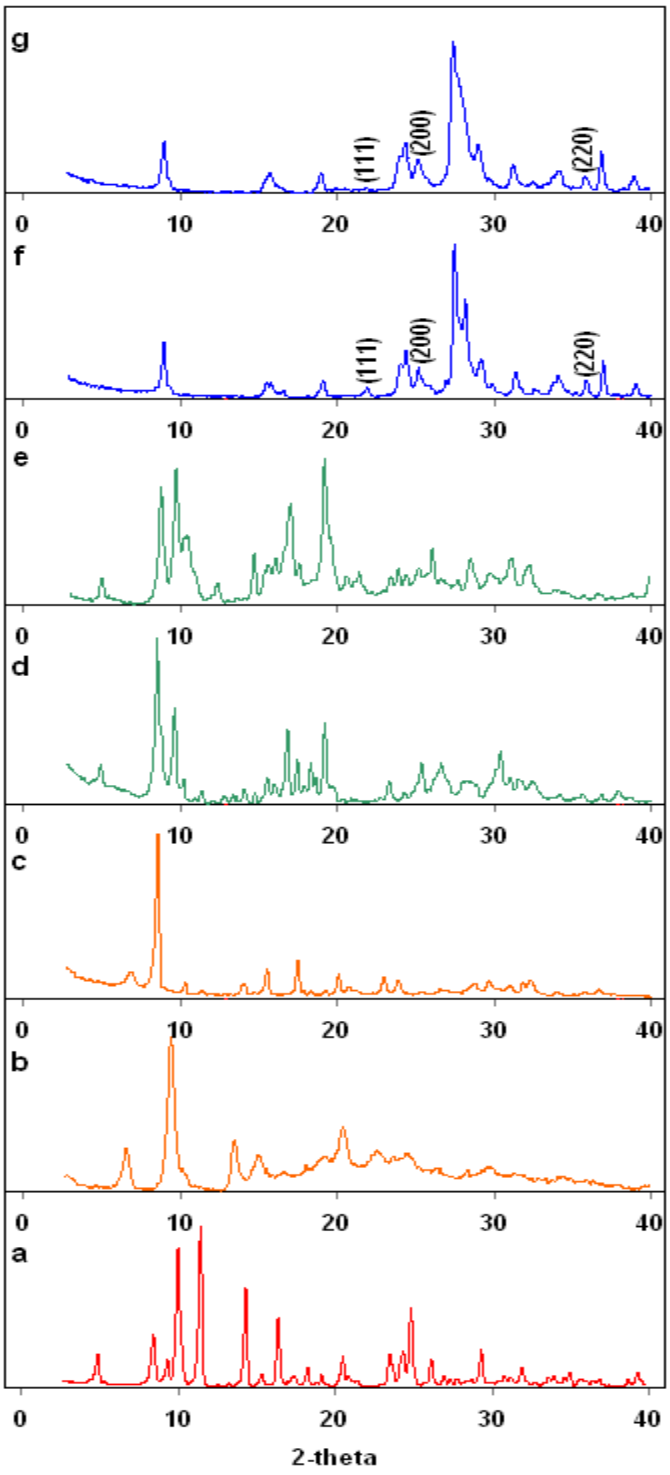

Figure S13. The XRD patterns of (a) compound **1** crystals, (b) compound **4** obtained after cation exchange with Li^+, (c) compound **4** after activation at 100 °C for 8 hours, (d) compound **5** obtained after cation exchange with Na^+, (e) compound **5** after activation at 100 °C for 8 hours, (f) compound **6** obtained after cation exchange with K^+ and (g) compound **6** after activation at 100 °C for 8 hours.

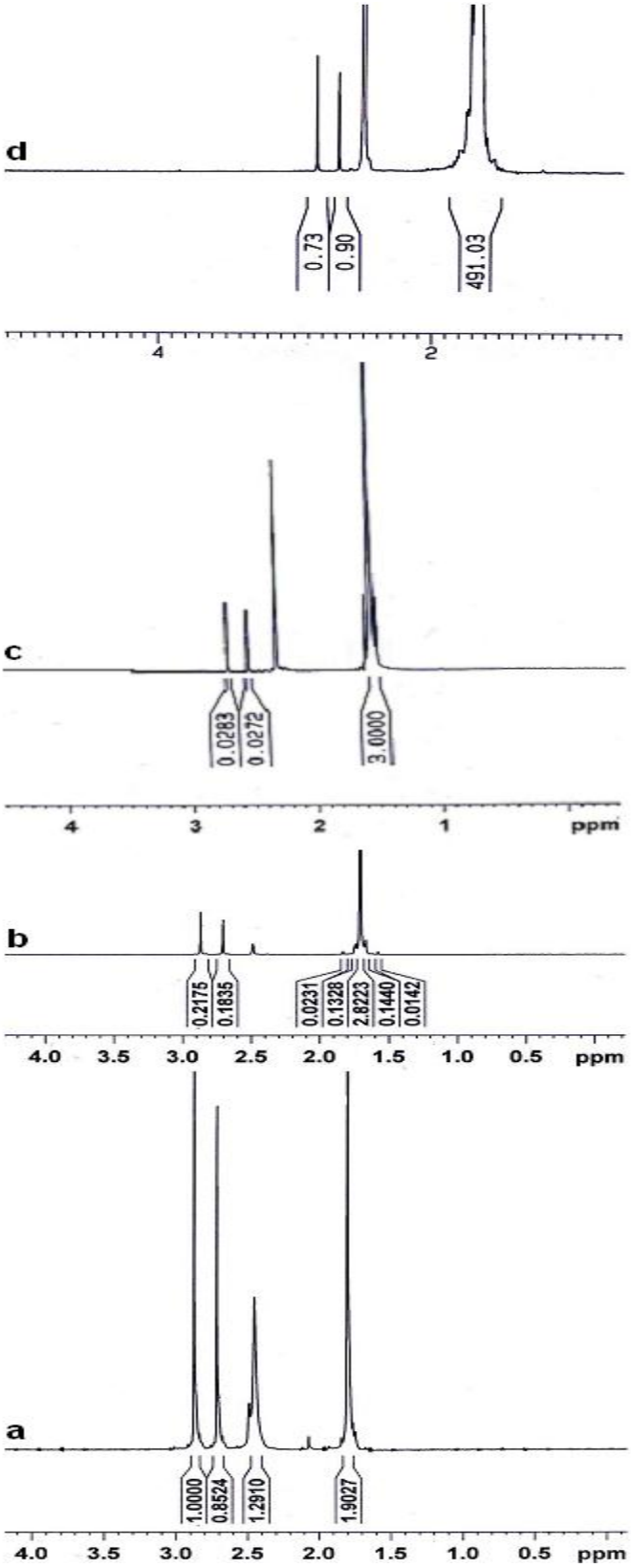

Figure S14. The ^{1}H-NMR spectra of compounds (a) **1**, (b) **4**, (c) **5** and (d) **6** after addition of 5 mg ammonium acetate to the NMR tube.

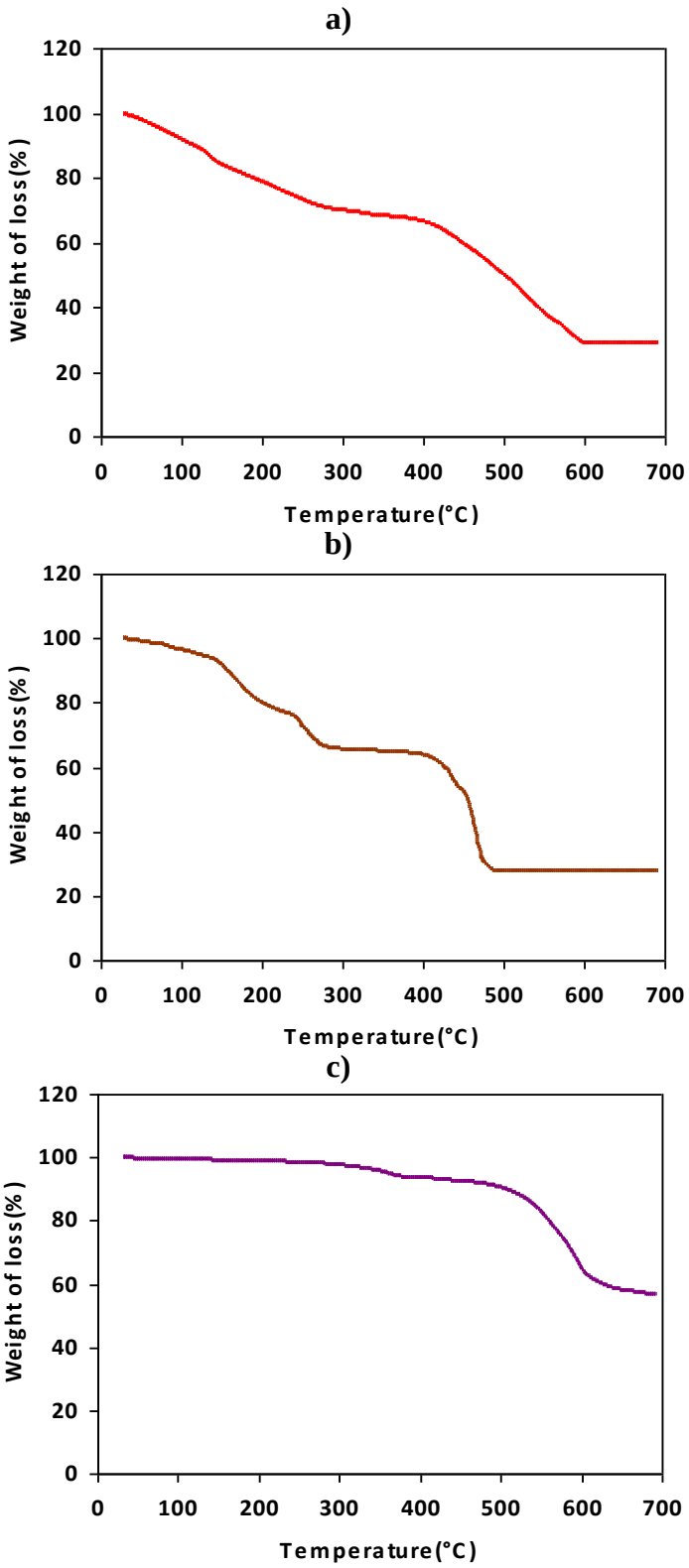

Figure S15. TGA curves of **4** (a), **5** (b) and **6** (c) MOF materials in a static atmosphere of nitrogen.

a)

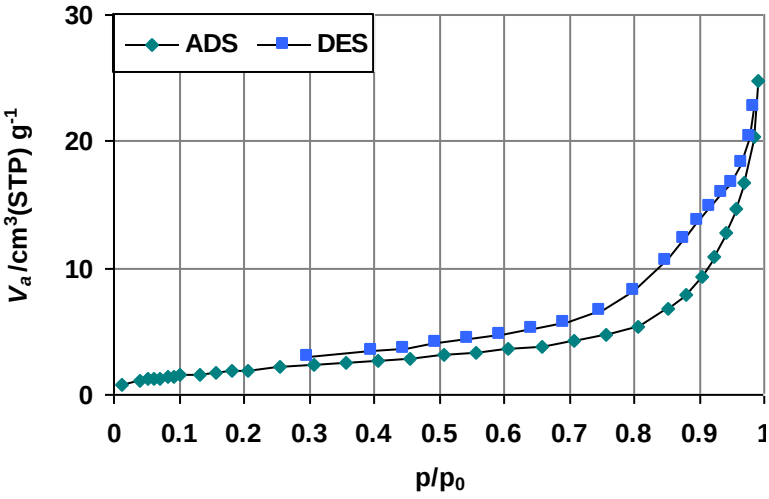
ADS
DES
V_a /cm^3(STP) g^{-1}
p/p$_0$

b)

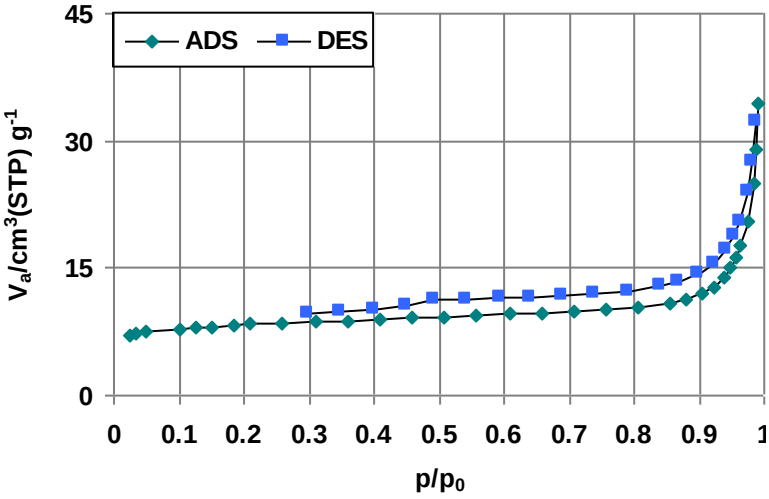
ADS
DES
V_a/cm^3(STP) g^{-1}
p/p$_0$

c)

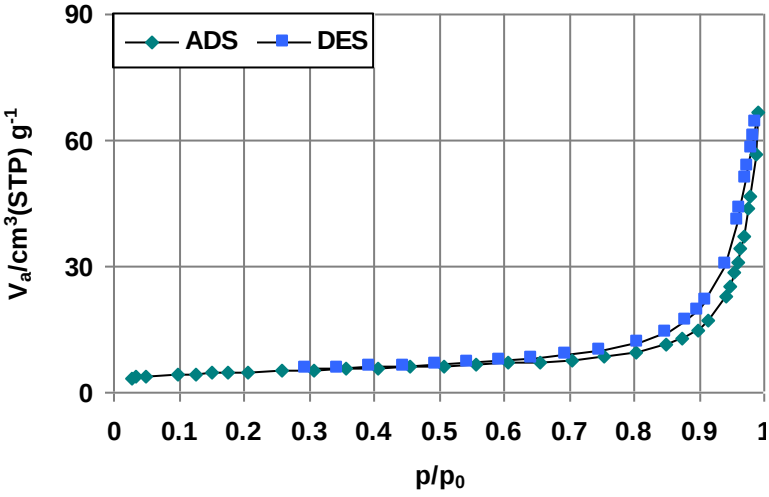
ADS
DES
V_a/cm^3(STP) g^{-1}
p/p$_0$

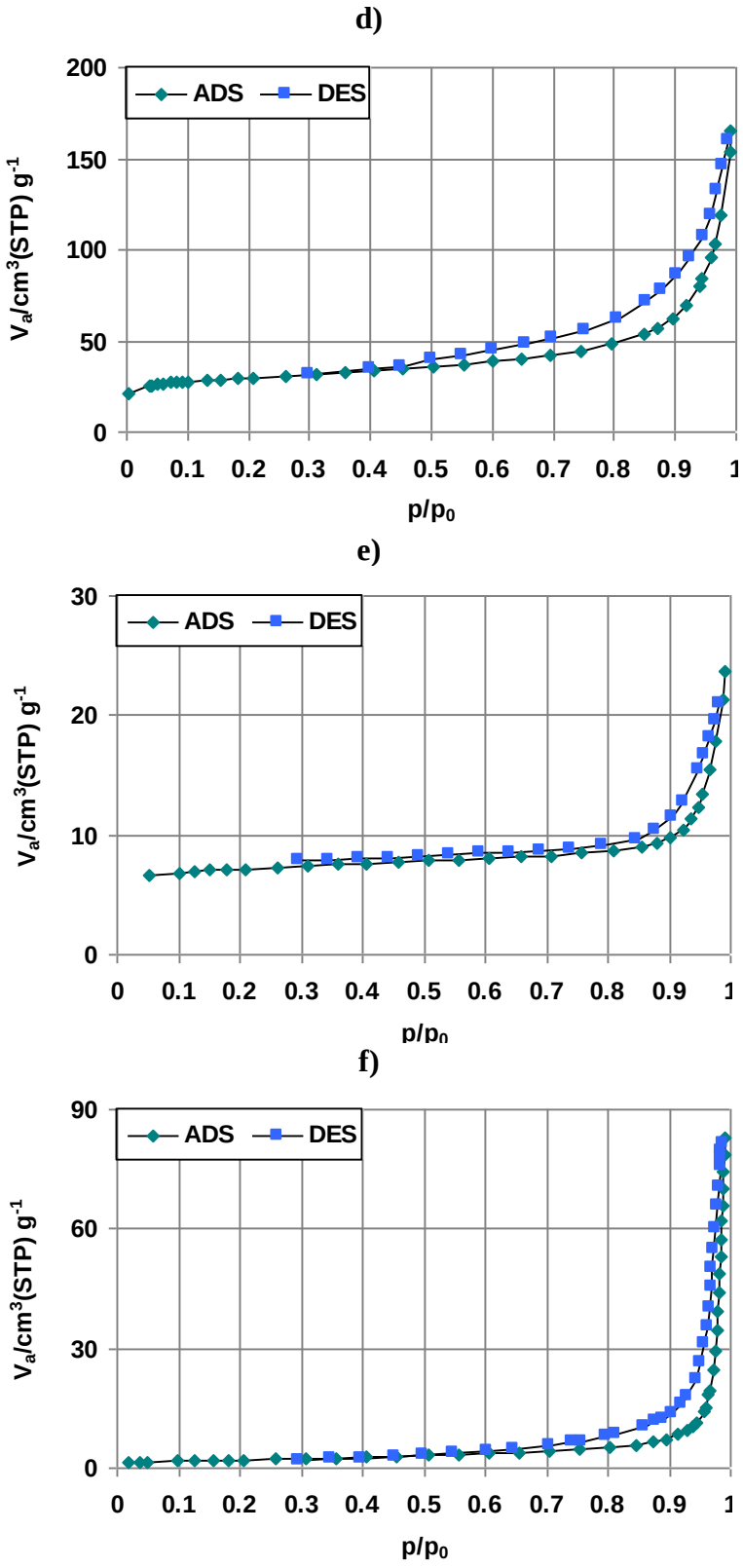

Figure S16. N_2 adsorption-desorption isotherms in **1** (a), **2** (b), **3** (c) **4** (d), **5** (e) and **6** (f) at 77K

Table S5. Structural properties and methane absorption capacities of **1-6** MOF materials at 1bar and 298 K.

MOF	van der Waals radii (Å)	N_2 gas sorption (cm^3(STP)/g at $P/P_0 = 1.0$)	S_{BET} ($m^2\ g^{-1}$)	$S_{Langmuir}$ ($m^2\ g^{-1}$)	CH_4 adsorption capacity (cm^3(STP)g^{-1})	CH_4 adsorption capacity (mmol g^{-1})
1	….	25	7.3	10.3	0.28	0.0125
2	Ni^{2+}: 1.63	34	30.3	38.7	1.31	0.0585
3	Cu^{2+}: 1.40	67	17.0	24.3	0.36	0.0161
4	Li^{+}: 1.82	166	109.2	137.5	2.27	0.1013
5	Na^{+}: 2.27	24	26.2	32.8	1.08	0.0482
6	K^{+}: 2.75	83	7.3	10.9	0.00	0.0000

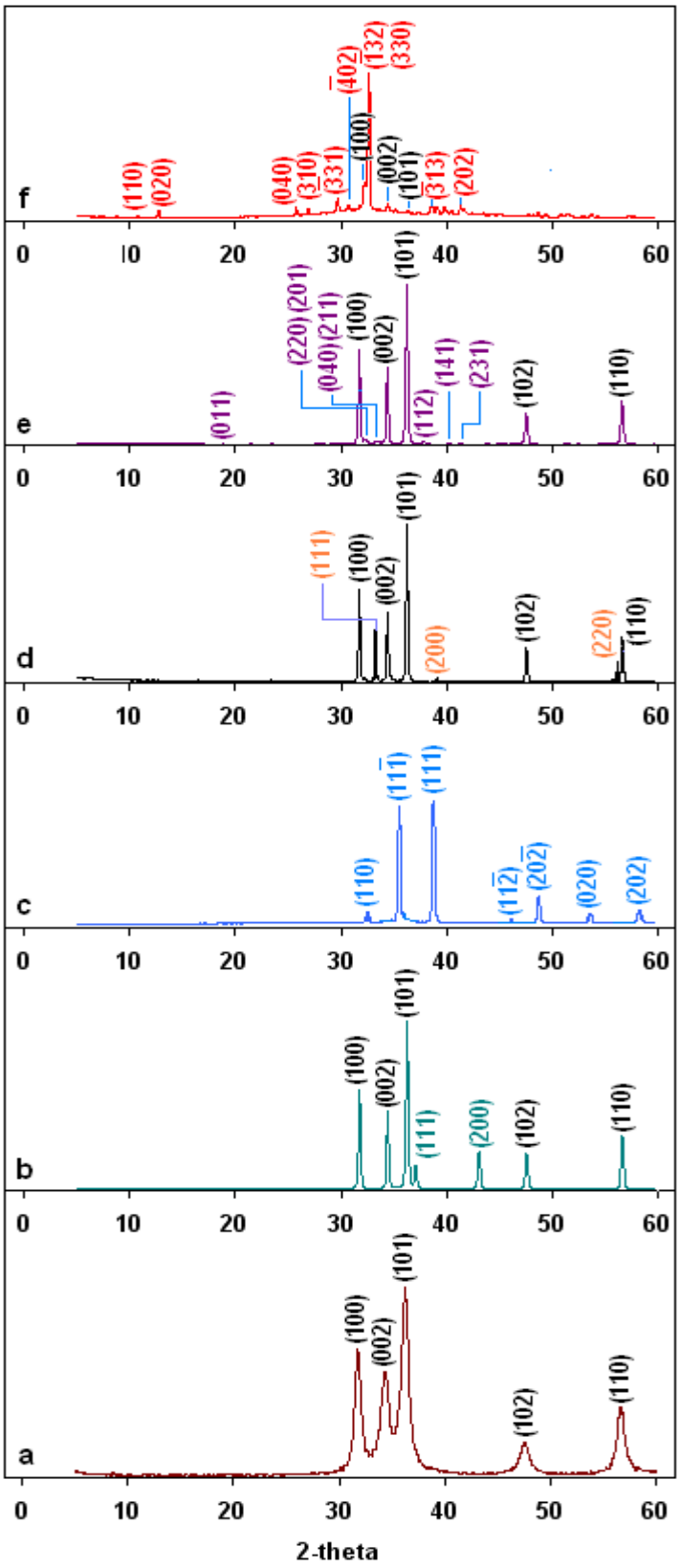

Figure S17. The XRD patterns of residue obtained after calcination of **1** (a), **2** (b), **3** (c) **4** (d), **5** (e) and **6** (f) MOF materials